

PAPER

## Facile fabrication of sensitivity-tunable strain sensors based on laser-patterned micro-nano structures

To cite this article: Shuo Zhang *et al* 2021 *J. Micromech. Microeng.* **31** 085003

View the [article online](#) for updates and enhancements.

### You may also like

- [Morphologically modulated laser-patterned reduced graphene oxide strain sensors for human fatigue recognition](#)  
Linna Mao, Tianxun Gong, Qinqin Ai *et al.*
- [High-performance strain sensor based on a 3D conductive structure for wearable electronics](#)  
Lei Zhang, Hairong Kou, Qiulin Tan *et al.*
- [An examination of scaling behavior in unstable epitaxial mound growth via kinetic Monte Carlo simulations](#)  
Joshua P Schneider, Dionisios Margetis, Frederic Gibou *et al.*





**IOP | ebooks™**

Bringing together innovative digital publishing with leading authors from the global scientific community.

Start exploring the collection—download the first chapter of every title for free.

# Facile fabrication of sensitivity-tunable strain sensors based on laser-patterned micro-nano structures

Shuo Zhang<sup>1,3</sup> , Wenjie Fei<sup>1,3</sup>, Qin Jiang<sup>1</sup>, Jiajun Jiang<sup>1</sup>, Kui Shi<sup>2</sup>, Longjian Xue<sup>2</sup> and Zhigang Wu<sup>1,\*</sup> 

<sup>1</sup> State Key Laboratory of Digital Manufacturing Equipment and Technology, School of Mechanical Science and Engineering, Huazhong University of Science and Technology, Wuhan 430074, People's Republic of China

<sup>2</sup> School of Power and Mechanical Engineering, Wuhan University, South Donghu Road 8, Wuhan 430072, People's Republic of China

E-mail: [zgwu@hust.edu.cn](mailto:zgwu@hust.edu.cn)

Received 31 January 2021, revised 25 May 2021

Accepted for publication 14 June 2021

Published 28 June 2021



## Abstract

Flexible/stretchable electronics have been well-developed in epidermal devices, wearable electronic systems and soft robotics for physiological signal detecting, real-time health monitoring and human-machine interfaces. As one of the most widespread-used transducers, strain sensors are playing a promising role in the developments of ongoing flexible electronics, especially equipped with tunable sensitivity (or gauge factor, GF). However, present investigations mainly focus on the enhancement of the sensitivity which required subtle designs or sophisticated fabrication processes. In this work, we report a facile fabrication strategy for configuring strain sensors with tunable sensitivity by adjusting the orientations and duty ratios of the micro-nano hierarchical Ag-coated microgrooves from laser patterning. The heterogeneous micro-nano structures enable localized large deformation to result in crack propagation on electrical layer during stretching, which endows the device with customized GF from 3.4 to 4570.6. The sensitivity-tunable strain sensor shows a great potential in monitoring various health conditions and voice recognition. This technique provides a facile and robust way to fabricate high-performance strain sensors for wearable physiological monitoring systems.

Supplementary material for this article is available [online](#)

Keywords: tunable sensitivity, orientation of microgrooves, duty ratio, strain sensor, flexible electronics

(Some figures may appear in colour only in the online journal)

## 1. Introduction

Stretchable and flexible electronics have greatly contributed to present smart intelligent systems [1, 2], wearable devices [3, 4] and epidermal electronics [5, 6] for sophisticated somatosensory detection [7, 8], physiological signal monitoring

[9–11] and human-machine interactions [12, 13], because of their flexibility/stretchability, and compatibility with human body [14]. As one of the most fundamental transducers, strain sensors were proposed for precisely exporting the variation of strain under deformation by consequently variable resistance.

Sensitivity is one of important performance metrics of strain sensors. To achieve high sensitivity of strain sensors, plenty of approaches have been developed to obtain elastomer composites and conductive nanomaterials, such as

<sup>3</sup> These authors contributed equally to this work.

\* Author to whom any correspondence should be addressed.

solution mixing [15–17], screen and inkjet printing [18–20], spraying coating [21–25] and chemical/physical vapor deposition [26–29] and so on. The composite increased the sensitivity of the strain sensor which can be used for detection of minute muscle movements such as artery pulses. However, the sensing mechanism of the composite is relatively complex. Strain sensors with high gauge factor (GF) are usually limited by the finite strain range and the linearity decreased under large strain, which makes it inappropriate for large motion detection, where a sensor with a larger strain range is preferred. However, it is a challenge to reach a balance between high sensitivity as well as good stretchability since strain sensors with high stretchability usually perform low sensitivity [30]. Some works could tune the sensitivity by adjusting the composition of the composite, but the fabrication process requires subtle steps. It is not convenient to manipulate sensors with sensitivity and the adjusting range is limited [31–35]. Thus, it is important to endow strain sensors with tunable sensitivity in a simple yet effective method.

UV-lasering process represents a convenient fabrication approach for the versatile and efficient creation of a patterned structure without extra molds or photomasks [36]. Complex micro-nano hierarchical structures can be formed by subtractive manufacturing according to programmed paths. When the laser is incident on an opaque substrate, the material will absorb part of the energy and undesired regions will be removed by selective laser ablation.

In this work, we reported a convenient method to turn a flat elastomeric polymer substrate towards a flexible strain sensor with tunable sensitivity. A facile procedure based on selective laser scanning was established to engrave a designed pattern onto an elastomeric polymer substrate surface and then coated with a thin silver film. The effect of surface topography on the flexible strain sensors was investigated in detail using stretching tests. Applications demonstrate the potential for a broad range of usages in epidermal electronics, over-strain alarm and surface shape measurement.

## 2. Experimental section

### 2.1. Materials and preparation

10 g silicone base and 1 g curing agent of PDMS (Sylgard 184, Dow Corning Corporation) mixed with 0.2 g carbon black (XC72R, CABOT, Alibaba, China) were employed as the deformed elastomeric polymer substrate with enhanced light absorbability. The carbon added PDMS (cPDMS) precursor was stirred at room temperature for 2 min and then degassed in a vacuum chamber for 10 min. The uncured cPDMS mixture was scraped on a polyethylene terephthalate plate with a film applicator (1000  $\mu\text{m}$ , Leaoqi) and then cured at 90 °C for 45 min in an oven (UF 55 plus, Memmert, Germany) as the flat substrate.

### 2.2. Fabrication of the flexible strain sensor

The surface topographies of grooves with different patterns were designed in AutoCAD (Autodesk, U.S.). As shown

in figure 1(a), designed patterns were engraved on the flat cPDMS substrate surface with a UV-laser marker (HGL-LSU3/5EI, Huagong Laser, China). After cleaning with isopropanol, the sample was loaded into thermal evaporation instrument system (BOX-RH400, SKY Technology Development Co., Ltd, CAS, China) for deposition of an Ag cathode (250 nm). In the end, copper wires were electrically connected to the conductive film using silver paste to assemble the strain sensor.

### 2.3. Surface characterization

The surface topographies, such as the three-dimensional (3D) profile, surface roughness ( $S_a$ ) and height difference, were measured by a 3D optical surface profiler (NewView 9000, ZYGO Corp., USA). The detailed micro surface morphology was observed by a field scanning electron microscope (FSEM, GeminiSEM300, Carl Zeiss, Jena, Germany). The constitution and purity were confirmed by element analysis using an ultra-high-resolution analytical FIB-SEM system (Helios NanoLab G3 CX, FEI Corp., Czech).

### 2.4. Electrical characterization

The sensor's resistance was measured by a Data Acquisition/Switch Unit (34 461A, KeySight Technologies). An oscilloscope (TBS 1202B-EDU, Tektronix, USA) was used to measure the voltage of the sensor in circuit for calculated resistance.

### 2.5. Finite element analysis

Three-dimensional finite element analysis allows the prediction of mechanical deformations and strain distributions of the simplified model by using COMSOL Multiphysics. A linear elastic model (Young's modulus, 750 kPa and Poisson's ratio, 0.49) was used to describe the elastomer's behaviour upon stretching.

### 2.6. Sensor preparation for demonstrations

In this work, for the fabrication of strain sensors (15  $\times$  30 mm) with different angle-designed patterns, the thickness of cPDMS was 800  $\mu\text{m}$ , the laser scanning speed was 200  $\text{mm s}^{-1}$ , hatch spacing was 50  $\mu\text{m}$ . FSEM images for element analysis have been added as figure S1 in the supporting information (available online at [stacks.iop.org/JMM/31/085003/mmedia](https://stacks.iop.org/JMM/31/085003/mmedia)). The results show that the Ag content increases with the increase of the thickness of Ag film. When the deposited thickness of Ag film was 50 nm or 150 nm, the Ag film was insulating because Ag cannot completely cover the surface with anisotropic microstructures and failed to form conductive pathways until the deposited thickness of Ag film was 250 nm. Therefore, the thickness of Ag film was chosen as 250 nm for the strain sensor. The strain sensors with designed pattern angle of 90° were used for bending performance tests, cyclic tensile tests, over-strain alarms and

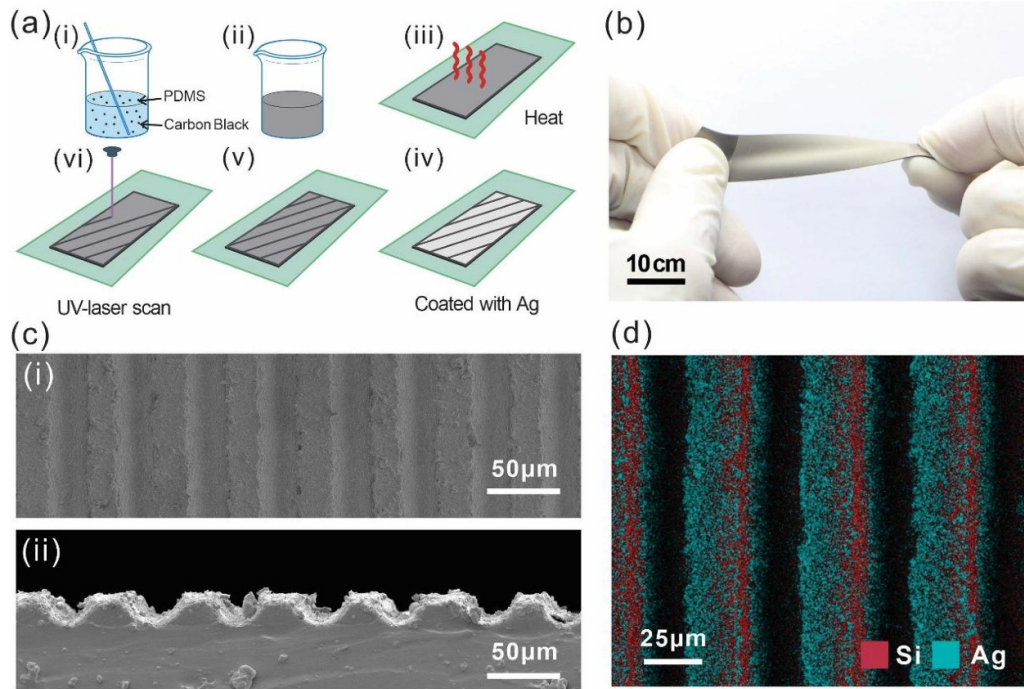


**Figure 1.** Fabrication process and photos/micrograph of the sensitivity-tunable strain sensor. (a) Schematic fabrication process of the flexible strain sensor. (b) Photography of the sensitivity-tunable strain sensor. (c) FSEM images of surface morphology of the sensitivity-tunable strain sensor, top view (i) and side view (ii). (d) Elements analysis of the top surface of the sensitivity-tunable strain sensor.

surface shape measurement. For health monitoring and voice recognition, the angle was chosen as  $0^\circ$  and the thickness of cPDMS substrate was  $200 \mu\text{m}$  to increase the adhesion to the epidermis. Besides, in order to meet the requirements for measurement accuracy, the copper wires were connected into a circuit and the voltage between two copper wires was detected using an oscilloscope. The change of the resistance could be recognized through the relation between resistance and voltage, equation (1), where  $R'$  is the resistance of the sensor,  $R$  is the resistance of the electrical resistance,  $E$  is the voltage of DC Power Supply and  $u$  is the voltage of the sensor

$$R' = \frac{Ru}{E - u}. \quad (1)$$

In the experiments of tunable sensing performance for strain sensors with different duty ratios-designed patterns, the hatch spacing was  $5 \mu\text{m}$ , the scanning speed was kept at  $200 \text{ mm s}^{-1}$  for one pass and the angle of the designed pattern was chosen as  $90^\circ$  for its unique linear relationship. To keep the electroconductibility, a thin layer Ag film ( $\sim 650 \text{ nm}$ ) was coated on the laser-scanned cPDMS surface.

### 3. Results and discussion

#### 3.1. Fabrication and surface characterization

Through Zhang's work [36], it has been discovered that un-melted particles spread due to the thermal gradient and generated triangle-shape-like microgrooves with

micro/nanostructures on the laser-scanned path. The designed patterns and uneven micro/nanostructures could be employed to achieve tunable sensitivity in strain sensors. What's more, the triangle-shape-like morphology makes it easy to deposit metal film on the sidewall of the microgrooves. Inspired by this finding, we fabricated a sensitivity-tunable strain sensor with different orientations and duty ratios of the microgrooves assisted by a UV-laser. Figure 1(a) schematically shows the fabrication processes of the sensitivity-tunable strain sensor and the photography of the fabricated sensor can be seen in figure 1(b). The top view shows the surface of laser-scanned cPDMS substrate, figure 1(c(i)). The side view of microgrooves was clearly shown in figure 1(c(ii)). Element analysis was used to characterize the component of the sensor. It can be found that the sensor is mainly composed of Si and Ag, which demonstrates that the Ag thin film is the conducting layer cover the elastomeric polymer substrate, figure 1(d).

The surface features of the strain sensor, e.g. roughness and morphology, were related to the designed pattern and the laser operational parameters. To further understand their relationship, the pattern was designed as lines and the hatch spacing of adjacent laser scanning lines ( $\Delta L$ , mm) was adjusted for different extensible structures. During the process, the laser scanning speed ( $v$ ,  $\text{mm s}^{-1}$ ) was adjusted to modify the laser's working parameters. As shown in figure 2(a), a 3D morphology of the sensor was measured by a 3D optical surface profiler, which also reveals the sensor's surface roughness ( $R_a$ ) and top surface morphology. The  $R_a$  of each sensor is determined by averaging three different scanning areas with a dimension of  $350 \times 350 \mu\text{m}^2$ , figure 2(b). On the condition

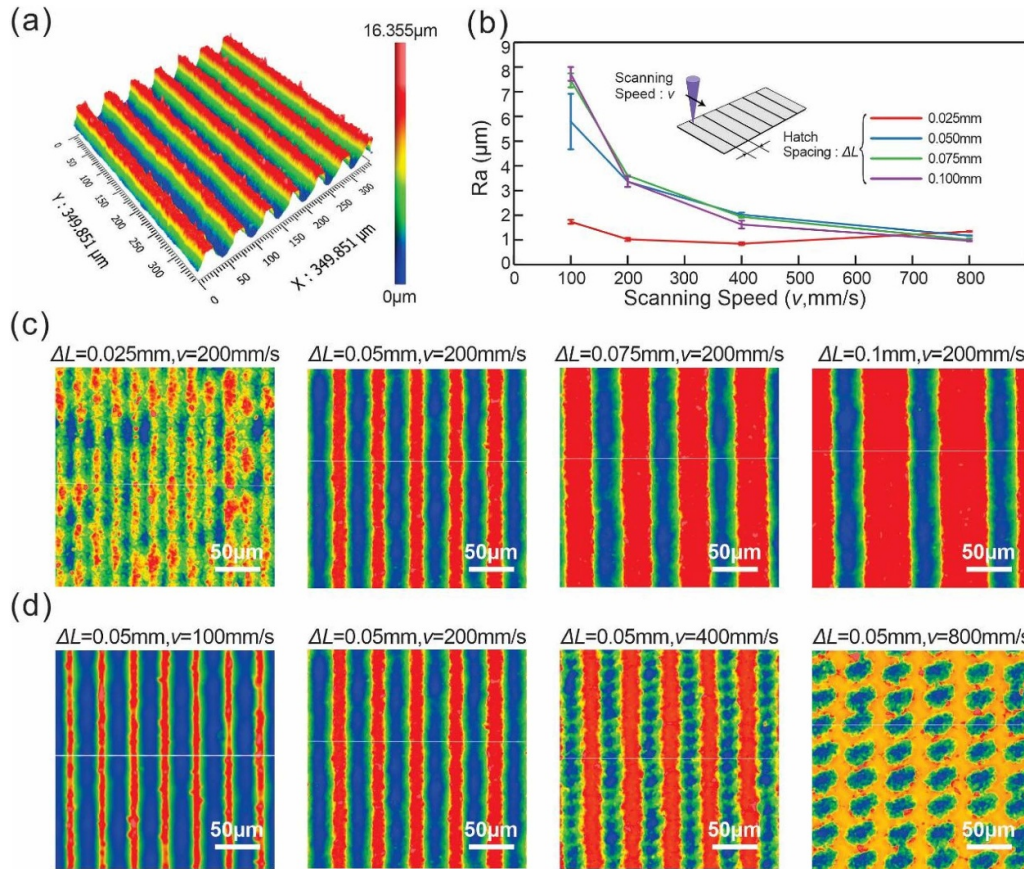


**Figure 2.** Surface morphology of the sensitivity-tunable strain sensor. (a) 3D morphology of the laser-scanned surface. (b) The surface roughness ( $R_a$ ) of laser-treated substrates under different scanning speed and hatch spacing. (c) The surface morphology of laser-scanned substrates under different hatch spacing. (d) The surface morphology of laser-scanned substrates under different scanning speeds.

that the hatch spacing was closed to the laser facula’s width ( $\sim 25 \mu\text{m}$ ), there is little variation of surface roughness at different scanning speeds, because the tracks became fluctuant and irregular-shaped and an unstable condition occurred. When the designed hatch spacing was more than the laser facula’s width ( $\sim 25 \mu\text{m}$ ), selective laser ablation removed materials from undesired regions and left a triangle groove on the surface, figure 2(c). Low scanning speed will increase the time interval between tracks, and relevantly promote the heat transfer from the present track to previously solidified materials, increasing the thermal gradient between tracks and further enhancing the intensity of humping [37]. If the scanning speed reached over  $400 \text{ mm s}^{-1}$ , hatch spacing has little effect on surface roughness. With the discontinuity of the track, it is difficult to recognize the direction of laser scanning beam, figure 2(d).

To further understand the effect of the designed pattern on the strain sensor’s sensitivity, hatch spacing was chosen as  $0.05 \text{ mm}$  and  $200 \text{ mm s}^{-1}$  for the laser scanning speed, which could guarantee complete line-shape pattern and concurrently save process time. The UV-laser process can be completed within 5 min in an ordinary laboratory environment for eight flexible strain sensors at once. The whole processing time was listed in table 1, which was 275 min approximately.

**Table 1.** Processing time estimation for a sensitivity-tunable flexible strain sensor.

Processing steps	Time (min)
Pattern plotting	5
cPDMS mixing	5
Degassing	10
cPDMS curing	45
UV laser treating	5
Cutting and cleaning samples	5
Depositing	180
Sticking copper wires	20
Total	275

### 3.2. Sensing mechanism

As shown in figure 3, FSEM images and schematic diagram have been employed to explain the sensor’s sensing mechanism. When the UV-laser scanned the substrate, uneven micro/nanostructures appeared on the scanning path. Figures 3(a(i)) and (b(i)) show FSEM images of the cross section of the cPDMS substrate before and after deposition. Figures 3(a(ii)–(iv)) and (b(ii)–(iv)) show the top view of the substrate under various strains, respectively. Notable

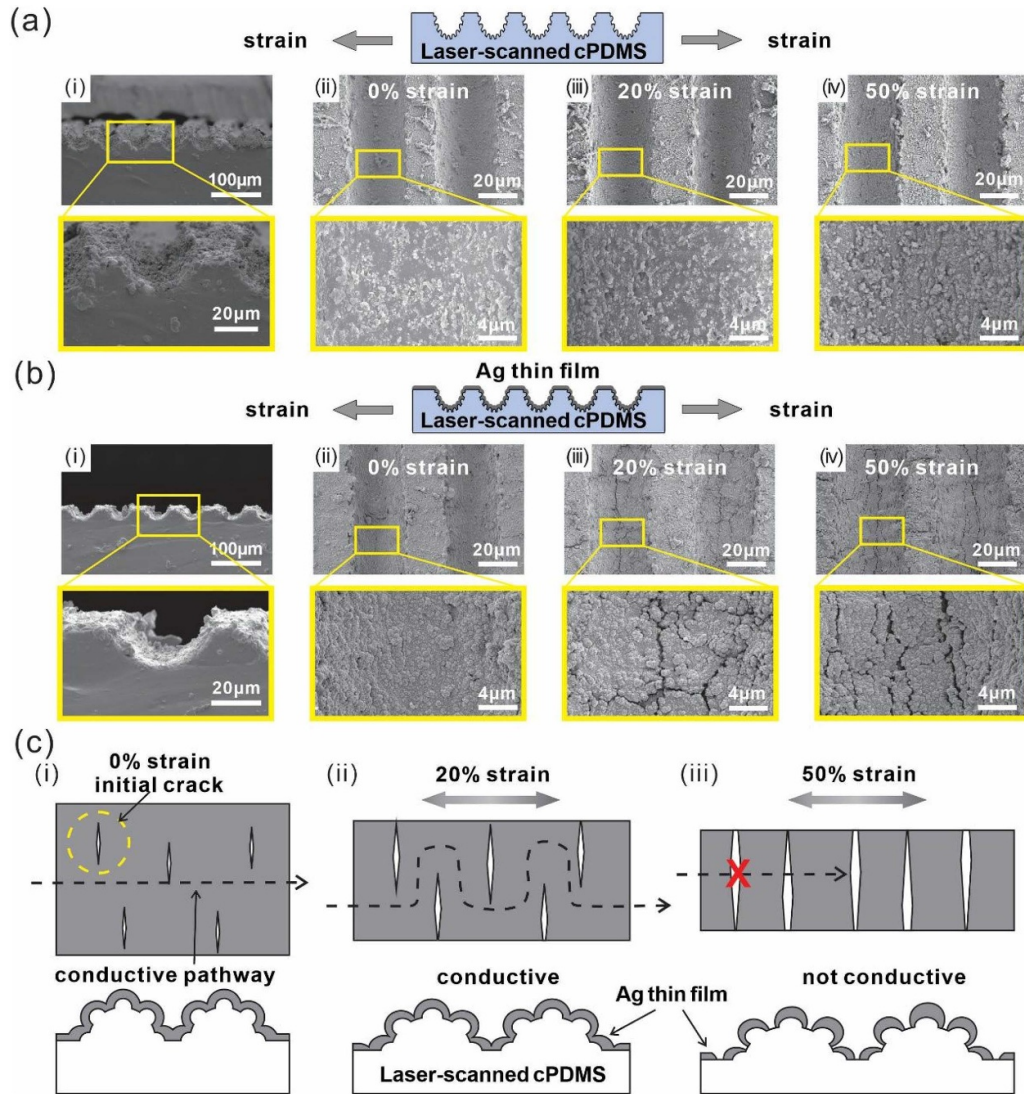


**Figure 3.** Sensing mechanism investigation. (a) FSEM images of pure cPDMS substrate and (b) FSEM images of Ag thin film ((i) for cross section and (ii) to (iv) for various strains). (c) Schematic diagram of crack propagation and conductive pathways upon stretching.

microcracks generated on the Ag thin film under strain mainly at the bottom of microgrooves that cannot be seen on the pure cPDMS substrate. This phenomenon was induced by the mismatch of Young's modulus between cPDMS substrate and Ag thin film. The sensor's sensing mechanism could be explained as crack propagation based on this effect. As shown in figure 3(c), anisotropic micro/nanostructures made microcracks sensitively originate and propagate in one specific direction along coated Ag thin film upon stretching. The opening and enlargement of microcracks critically limited the electrical conduction of Ag thin films upon stretching. Consequently, conductive pathways were blocked and the overall electrical resistance of Ag film increased in one specific direction. It can be concluded that the resistance of the sensor experienced a relative increase as the applied strain increased. However, when all the conductive pathways blocked by microcracks, the Ag film turned into a non-conducting state as the result of a large strain [20, 29]. When the strain was

released, microcracks recovered to initial conditions and pathways returned to the conductive state.

### 3.3. Tunable sensitivity of strain sensors

During the laser scanning, the scanning speed ( $v$ ,  $\text{mm s}^{-1}$ ) and hatch spacing of adjacent laser scanning lines ( $\Delta L$ ,  $\text{mm}$ ) can be adjusted to affect the patterning behaviours and further influence the obtained surface morphology. When the scanning speed and hatch spacing were selected, the size of the microgroove was determined. In this condition, different pattern designs engraved on the surface of the substrate were supposed to have an influence on the conductive pathways and thus the sensitivity of obtained strain sensors.

As shown in the inset of figure 4(a), the angle between the microgroove and the stretching direction was designed with different values ( $0^\circ$ ,  $30^\circ$ ,  $60^\circ$ ,  $90^\circ$ ). In the tensile testing, the

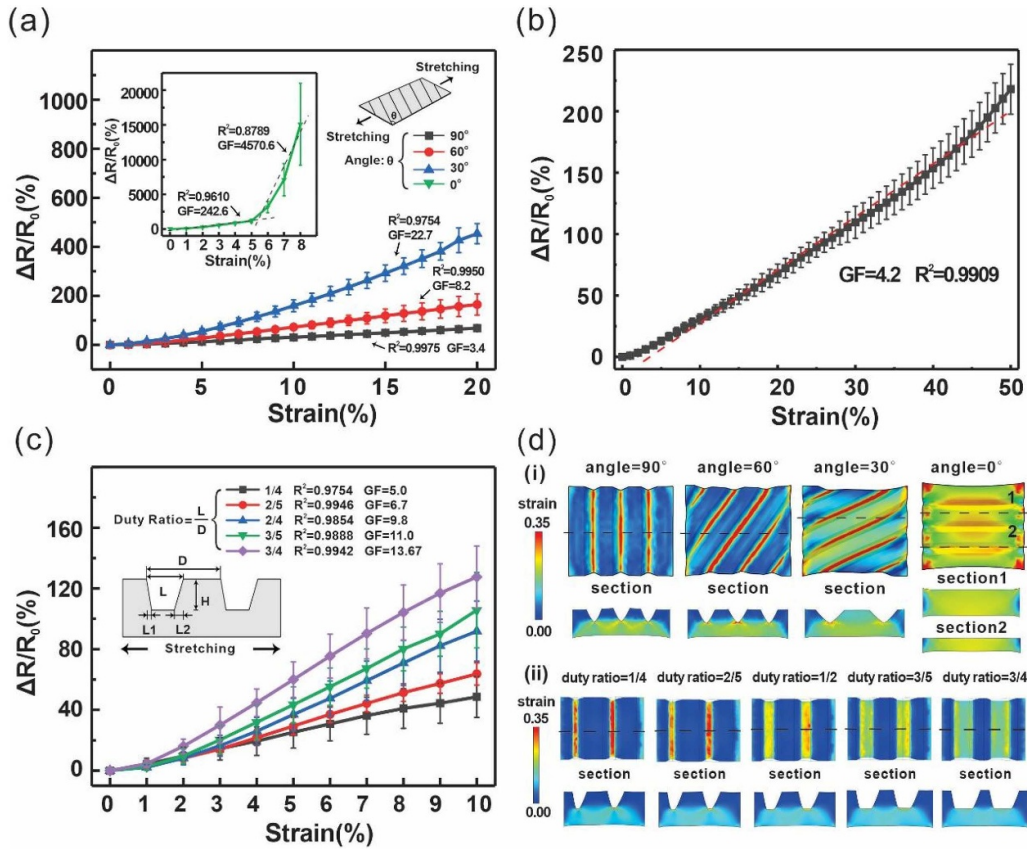


**Figure 4.** Tunable strain sensing performances. (a) The relative resistance change along the variation of the angle. (b) The relative resistance change along tensile strain up to 50%. (c) The relative resistance change along the duty ratio. (d) Finite element analysis of the strain distribution for sensors to tensile strains with different (i) angle-designed and (ii) duty ratio-designed surface morphologies.

resistance of the electrode was measured using a data acquisition/switch unit. The change in resistance of the electrode during substrate stretching can be expressed as  $\Delta R$ ,  $\Delta R = R - R_0$ , where  $R_0$  is the initial resistance under no strain and  $R$  is the resistance under various strains. The GF ( $GF = (\Delta R/R_0)/\epsilon$ ) was calculated to describe the sensitivity of the sensors. As shown in figure 4(a), the resistance of the sensor increased as a result of various strains. It can be noted that the strain sensor with different designed angle present different performance. When the angle was 90°, the GF was 3.4, while the GF can be up to 4570.6 when the angle decreased to 0°. The coefficient of determination ( $R^2$ ) for the angle of 90°, 60° and 30° were 0.9975, 0.9950 and 0.9754, respectively, within 20% strain, showing a good linear relationship. The sensor with the angle of 0° had two linear regions which possessed GFs as high as 242.6 ( $\epsilon < 5\%$ ) and 4570.6 ( $5\% < \epsilon < 8\%$ ) and the coefficient of determination was 0.9610 and 0.8789 respectively. Further, the sample of 90° angle can be stretched up to 50% strain and still kept conductive with a good linear relationship, figure 4(b), which make it suitable for large deformation detection. Through the simulation result in figure 4(d(i)), it is suggested that stresses concentrate mainly at the bottom of the microgrooves, which was corresponded to the FSEM images in figures 3(b(iii)) and (b(iv)). The relationship between the sensitivity and angle could be explained as: at the angle of 90°, a microcrack at the bottom cannot extend to whole length

of the microgroove within tiny strain; while at the angle of 0°, a microcrack at the bottom can extend to whole width of the microgroove within tiny strain which block the conductive pathway obviously; hence, the sensor designed with lower angle could bear larger stretching and it can be concluded that the sensor's sensitivity increased with the decrease of the angle. Consequently, different angle led to broad-range sensitivity, which has potential for various applications.

Furthermore, when the hatch spacing was less than the laser facula's width ( $\sim 25 \mu\text{m}$ ), sufficient overlaps between the tracks were favourable to form a relatively flat surface. This made it possible to design complicated surface morphology. When the hatch spacing was  $5 \mu\text{m}$ , intensive tracks reinforced thermal effect, which caused more thickness loss of cPDMS. To further investigate the influence of structural design on the sensitivity of flexible strain sensors, the resulting surface topography (figure S2) was studied by five parameters: the depth  $H$  of the engraved groove, the distance  $D$  between neighboring engraved microgrooves, the top width  $L$  of the engraved microgroove, and the bottom width  $L_2$  and  $L_3$  of the engraved microgroove, which were all labeled in table S1. Through a statistical analysis,  $L$  increase with more scanning lines while the depth had no significant change. Referring to the above finding, surface morphology can be designed into different duty ratios ( $= L/D$ ) with the same distance ( $D$ ), such as 1/4, 2/5, 2/4, 3/5 and 3/4. The simulation result of different

**Table 2.** Summary of the performance of sensitivity-tunable strain sensors reported.

Reference	Stretchability (%)	Gauge factor	Linearity	Preparation time
[31]	70%	2–14	Linear	>7 h
[32]	260%	4.5–70	Nonlinear	>4.5 h
[33]	0.8%	0.61–6.42	Linear	Not mentioned
[34]	130%	4.4–772.6	Nonlinear	>30 h
[35]	1%	18.60–290.62	Nonlinear	Not mentioned
This work	50%	3.4–4570.6	Linear	4.6 h

duty ratios has been shown in figure 4(d(ii)), from which we can find that stresses mainly concentrate at the bottom of the microgrooves. The experiment result has been shown in figure 4(c). When the duty ratio increased from 1/4 to 3/4, the sensitivity achieved higher and the GF ranged from 5.0 to 13.67 with good linearity. Higher duty ratios indicate more laser-scanned areas and more micro/nanostructures on the surface of the substrate which could make more cracks under similar strain levels and enhance the sensitivity of the strain sensor.

A summary of performance results of recently sensitivity-tunable strain sensors has been reported in table 2. Compared to many other available techniques, the experiment results effectively demonstrate selective laser ablation as a convenient technique for rapid prototyping of sensitivity-tunable strain sensors.

### 3.4. Bending sensor test

To meet the requirement for wearable devices, the bending performance of the fabricated sensor was further tested. The surface-structured cPDMS composite film was mechanically bent using a tensile testing machine. The bending radius was calculated through post-processing. Figures 5(a) and (b) show the relative change in resistance at different bending radius. When the sensor was bent outwards, figure 5(a), the sensor performed as stretched. As a result, the resistance increased with the decrease of the bending radius. On the contrary, when the sensor was bent inwards, figure 5(b), adjacent Ag particles contacted each other and the conductivity increased which performed as a decrease of resistance.

Furthermore, a cyclic tensile test with 1000 cycles was performed, figure 5(c). In the subsequent stable stage, there is no apparent fluctuation and the resistance change was almost the same as each cycle. The cracking under strain and release were reversible, which explained the high durability of this strain sensor.

### 3.5. Demonstrations for different requirements of sensitivity

The sensitive strain sensor can be used as wearable devices for health monitoring. Wrist pulse is a significant physiological indicator for determining arterial blood pressure and heart-beat. As shown in figure 6(a), the sensor was mounted on

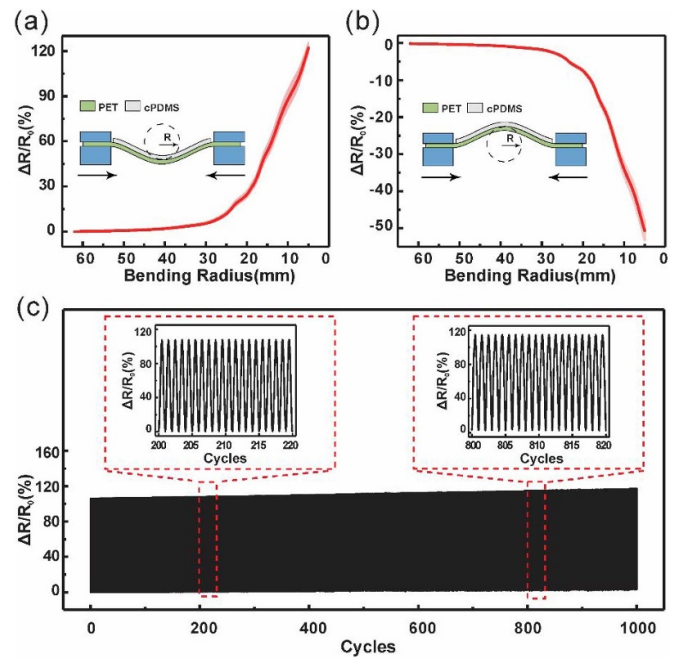


**Figure 5.** Sensing performances under bending and cyclic test under strain up to 20%. (a) The relative resistance change of sensors when bent inwards. (b) The relative resistance change of sensors when bent outwards. The inset shows the bending process and calibration of the radius. (c) Mechanical test under a strain of 20% for 1000 cycles.

the volunteer’s wrist. When the volunteer caught a cold, the pulse was weak and was difficult to be detected by the sensor. The single collected by the same volunteer under health status demonstrated a regular pulse shape with a heart rate of ~75 beats per minute (bpm). Generally, each cycle of pulse rate has three characteristic peaks: percussion (P), tidal (T), and diastolic (D) [38]. After exercise, the volunteer’s pulse was racing and the amplitude of the signal became greater than normal.

A sensor was attached to the throat of the volunteer. When the volunteer spoke several words, such as ‘hello’, ‘how’, ‘are’, and ‘you’, the sensor recorded specific patterns (figure 6(b)) by the value of  $\Delta R/R_0$  for each phonation. Each word resulted in distinct movements of the laryngeal prominence and the sensor responded with distinguishing different signals. The same patterns were produced when the words were repeated, suggesting the sensor’s reliability for use as voice recognition.

The reversibility and stretchability of strain sensors displayed the possible application as an over-strain alarm. As shown in figure 6(c), a strain sensor with 90° designed pattern was connected to a light-emitting diode (LED) in series provided with a suitable source voltage. In the beginning, the sensor performed as a conducting wire when the LED was lit. When the sensor was stretched, the light turned dim. Once exceeding a critical strain of over 50%, the sensor switched to a failure state and the LED went out suddenly. When the strain was released, the circuit returned to connection and the LED lit again. The LED’s extinguishment could be recognized as an alarm signal and the sensor protected the circuit from critical strains.



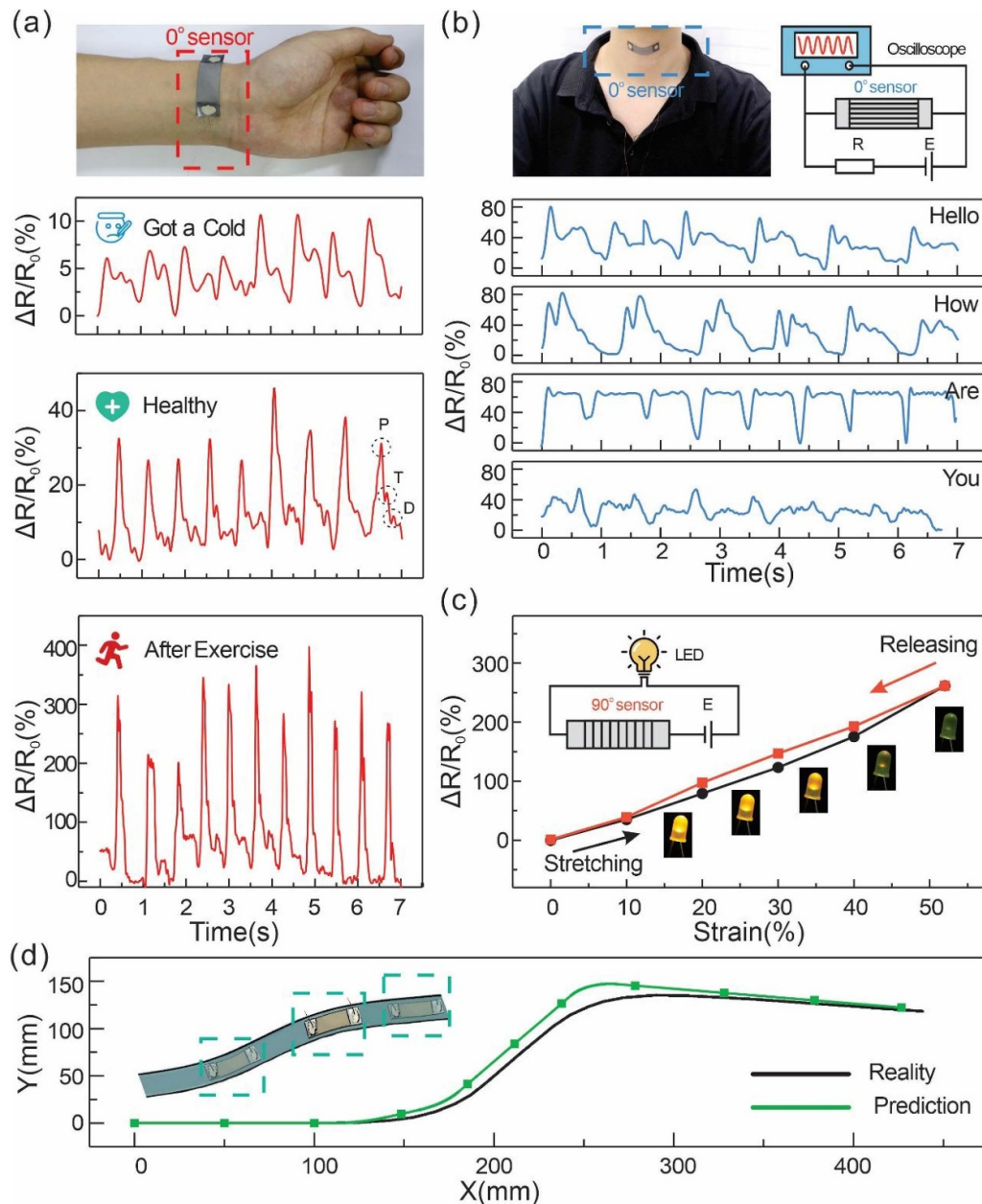


**Figure 6.** Application demonstrations. (a) Detection of the pulse signal under different condition. (b) The skin-attachable voice recognition. (c) Protective functions of the sensor in a circuit against a critical strain. (d) Surface shape measurement.

When the sensor was bent at different orientations, the relative change of the resistance has different performance. The resistance increased when the sensor was bent outwards and decreased when bent inwards. As a result, the sensor can be used to detect the degree of a curved surface. As shown in figure 6(d), the arc length of the laser-scanned part was 30 mm and the length of the part connected to the copper wire was 10 mm on each side. When the sensor was attached to different parts of a curved track, the change of resistance was recorded and then turned into the deformation curvature. Adjacent sensors were supposed to have the same or opposite bending orientation. Two different conditions were discussed in the tables S2 and S3. Through the formula, the shape of each part of the track can be predicted. Figure 4(d) shows the predicted

result and actual shape of the track. The position error of the ending spot was guaranteed within 15 mm which indicated the potential application in surface shape measurement for soft robotics.

#### 4. Summary

In this work, a method for sensitivity-tunable strain sensor is proposed by combining laser ablation and Ag deposition on the cPDMS substrate. Selective laser ablation is established as a convenient fabrication approach to create different surface topography on elastomeric polymer substrate at different scanning speeds and hatch spacing which could be

adjusted to tune the electrical performances of the sensors. The micro/nanostructures on the laser-scanned surface made cracks originate and propagate upon stretching as sensing mechanism. The fabricating process of strain sensors provides a new way to develop sensors with tunable GF ranging from 3.4 to 4570.6 under larger strain which has a great potential in wearable electronic devices.

### Data availability statement

All data that support the findings of this study are included within the article (and any supplementary files).

### Acknowledgments

This work is supported by the National Natural Science Foundation of China (No. U1613204). The authors would also like to acknowledge the support of the Analytic Testing Center and the Flexible Electronics Research Center of the HUST.

### ORCID iDs

Shuo Zhang  <https://orcid.org/0000-0002-0818-8955>  
Zhigang Wu  <https://orcid.org/0000-0002-3719-406X>

### References

- [1] Zhang H, Lan Y, Qiu S, Min S, Jang H, Park J, Gong S and Ma Z 2021 Flexible and stretchable microwave electronics: past, present, and future perspective *Adv. Mater. Technol.* **6** 2000759
- [2] Niu S *et al* 2019 A wireless body area sensor network based on stretchable passive tags *Nat. Electron.* **2** 361–8
- [3] Zhao J *et al* 2019 A fully integrated and self-powered smartwatch for continuous sweat glucose monitoring *ACS Sens.* **4** 1925–33
- [4] Heo J S, Eom J, Kim Y and Park S K 2018 Recent progress of textile-based wearable electronics: a comprehensive review of materials, devices, and applications *Small* **14** 1703034
- [5] Wang Y *et al* 2020 Epidermal electrodes with enhanced breathability and high sensing performance *Mater. Today Phys.* **12** 100191
- [6] Kim D and Rogers J A 2011 Epidermal electronics *Science* **371** 838–43
- [7] Chang Y, Wang L, Li R, Zhang Z, Wang Q, Yang J, Guo C F and Pan T 2020 First decade of interfacial iontronic sensing: from droplet sensors to artificial skins *Adv. Mater.* **22** 2003464
- [8] Wan Y *et al* 2018 Natural plant materials as dielectric layer for highly sensitive flexible electronic skin *Small* **14** 1801657
- [9] Yao S and Zhu Y 2014 Wearable multifunctional sensors using printed stretchable conductors made of silver nanowires *Nanoscale* **6** 2345
- [10] Lo Presti D, Massaroni C, D'Abbraccio J, Massari L, Caponero M, Longo U G, Formica D, Oddo C M and Schena E 2019 Wearable system based on flexible FBG for respiratory and cardiac monitoring *IEEE Sens. J.* **19** 7391–8
- [11] Gao W *et al* 2016 Fully integrated wearable sensor arrays for multiplexed *in situ* perspiration analysis *Nature* **529** 509–14
- [12] He T, Sun Z, Shi Q, Zhu M, Anaya D V, Xu M, Chen T, Yuce M R, Thean A V and Lee C 2019 Self-powered glove-based intuitive interface for diversified control applications in real/cyber space *Nano Energy* **58** 641–51
- [13] He Q, Wu Y, Feng Z, Sun C, Fan W, Zhou Z, Meng K, Fan E and Yang J 2019 Triboelectric vibration sensor for a human-machine interface built on ubiquitous surfaces *Nano Energy* **59** 689–96
- [14] Rogers J A, Someya T and Huang Y 2010 Materials and mechanics for stretchable electronics *Science* **327** 1603–7
- [15] Li T, Li J, Zhong A, Han F, Sun R, Wong C, Niu F, Zhang G and Jin Y 2020 A flexible strain sensor based on CNTs/PDMS microspheres for human motion detection *Sens. Actuators A* **306** 111959
- [16] Zheng Y, Li Y, Dai K, Wang Y, Zheng G, Liu C and Shen C 2018 A highly stretchable and stable strain sensor based on hybrid carbon nanofillers/polydimethylsiloxane conductive composites for large human motions monitoring *Compos. Sci. Technol.* **156** 276–86
- [17] Liu H, Li Y, Dai K, Zheng G, Liu C, Shen C, Yan X, Guo J and Guo Z 2016 Electrically conductive thermoplastic elastomer nanocomposites at ultralow graphene loading levels for strain sensor applications *J. Mater. Chem. C* **4** 157–66
- [18] Muth J T, Vogt D M, Truby R L, Mengüç Y, Kolesky D B, Wood R J and Lewis J A 2014 Embedded 3D printing of strain sensors within highly stretchable elastomers *Adv. Mater.* **26** 6307–12
- [19] Lee C, Jug L and Meng E 2013 High strain biocompatible polydimethylsiloxane-based conductive graphene and multiwalled carbon nanotube nanocomposite strain sensors *Appl. Phys. Lett.* **102** 183511
- [20] Tolvanen J, Hannu J and Jantunen H 2018 Stretchable and washable strain sensor based on cracking structure for human motion monitoring *Sci. Rep.* **8** 13210–41
- [21] Obitayo W and Liu T 2015 Effect of orientation on the piezoresistivity of mechanically drawn single walled carbon nanotube (SWCNT) thin films *Carbon* **85** 372–82
- [22] Lipomi D J, Lee J A, Vosgueritchian M, Tee B C K, Bolander J A and Bao Z 2011 Electronic properties of transparent conductive films of PEDOT:PSS on stretchable substrates *Chem. Mater.* **24** 373–82
- [23] Park J J, Hyun W J, Mun S C, Park Y T and Park O O 2015 Highly stretchable and wearable graphene strain sensors with controllable sensitivity for human motion monitoring *ACS Appl. Mater. Interfaces* **7** 6317–24
- [24] Xu M, Li X, Jin C, He Z and Zhang Q 2020 High-performance epidermal strain sensor based on macro-defect graphene foams *Sens. Actuators A* **303** 111721
- [25] Roh E, Hwang B, Kim D, Kim B and Lee N 2015 Stretchable, transparent, ultrasensitive, and patchable strain sensor for human-machine interfaces comprising a nanohybrid of carbon nanotubes and conductive elastomers *ACS Nano* **9** 6252–61
- [26] Zou Q, Zheng J, Su Q, Wang W, Gao W and Ma Z 2019 A wave-inspired ultrastretchable strain sensor with predictable cracks *Sens. Actuators A* **300** 111658
- [27] Yang T, Jiang X, Zhong Y, Zhao X, Lin S, Li J, Li X, Xu J, Li Z and Zhu H 2017 A wearable and highly sensitive graphene strain sensor for precise home-based pulse wave monitoring *ACS Sens.* **2** 967–74
- [28] Wu Y, Liu H, Chen S, Dong X, Wang P, Liu S, Lin Y, Wei Y and Liu L 2016 Channel crack-designed Gold@PU sponge for highly elastic piezoresistive sensor with excellent detectability *ACS Appl. Mater. Interfaces* **9** 20098–105
- [29] Ko E, Kim H, Lee S, Kim T and Kim H 2017 Stretchable Ag electrodes with mechanically tunable optical transmittance on wavy-patterned PDMS substrates *Sci. Rep.* **7** 46739
- [30] Tao L, Wang D, Tian H, Ju Z, Liu Y, Pang Y, Chen Y, Yang Y and Ren T 2017 Self-adapted and tunable graphene strain

- sensors for detecting both subtle and large human motions *Nanoscale* **9** 8266–73
- [31] Amjadi M, Pichitpajongkit A, Lee S, Ryu S and Park I 2014 Highly stretchable and sensitive strain sensor based on silver nanowire–elastomer nanocomposite *ACS Nano* **8** 5154–63
- [32] Yang S, Li C, Cong T, Zhao Y, Xu S, Wang P and Pan L 2019 Sensitivity-tunable strain sensors based on carbon nanotube@carbon nanocoil hybrid networks *ACS Appl. Mater. Interfaces* **11** 38160–8
- [33] Wang X, Sparkman J and Gou J 2017 Strain sensing of printed carbon nanotube sensors on polyurethane substrate with spray deposition modeling *Compos. Commun.* **3** 1–6
- [34] Cai Y, Shen J, Ge G, Zhang Y, Jin W, Huang W, Shao J, Yang J and Dong X 2018 Stretchable Ti3 C2 Tx MXene/carbon nanotube composite based strain sensor with ultrahigh sensitivity and tunable sensing range *ACS Nano* **12** 56–62
- [35] Lee G, Kim M, Min S, Kim H, Kim H, Keller R, Ihn J and Ahn S 2019 Highly sensitive solvent-free silver nanoparticle strain sensors with tunable sensitivity created using an aerodynamically focused nanoparticle printer *ACS Appl. Mater. Interfaces* **11** 26421–32
- [36] Zhang S, Jiang Q, Xu Y, Guo C F and Wu Z 2020 Facile fabrication of self-similar hierarchical micro-nano structures for multifunctional surfaces via solvent-assisted UV-laser *Micromach.-Basel* **11** 682
- [37] Guo C, Li S, Shi S, Li X, Hu X, Zhu Q and Ward R M 2020 Effect of processing parameters on surface roughness, porosity and cracking of as-built IN738LC parts fabricated by laser powder bed fusion *J. Mater. Process. Technol.* **285** 116788
- [38] Yang T, Li X, Jiang X, Lin S, Lao J, Shi J, Zhen Z, Li Z and Zhu H 2016 Structural engineering of gold thin films with channel cracks for ultrasensitive strain sensing *Mater. Horiz.* **3** 248–55